Biosensors and Bioelectronics 26 (2010) 689–695

Contents lists available at ScienceDirect

Biosensors and Bioelectronics

journal homepage: www.elsevier.com/locate/bios

Simultaneous electrochemical determination of superoxide anion radical and nitrite using Cu,ZnSOD immobilized on carbon nanotube in polypyrrole matrix

Seenivasan Rajesh[a], Anantha Koteswararao Kanugula[b], Kalpana Bhargava[c], Govindaswamy Ilavazhagan[c], Srigiridhar Kotamraju[b], Chandran Karunakaran[a,*]

[a] Biomedical Research Laboratory, Department of Chemistry, VHNSN College, Virudhunagar 626 001, Tamil Nadu, India
[b] Center for Chemical Biology, Indian Institute of Chemical Technology, Hyderabad 500 607, India
[c] Peptide and Proteomics Division, Defence Institute of Physiology and Allied Sciences (DIPAS), New Delhi 110 054, India

ARTICLE INFO

Article history:
Received 19 March 2010
Received in revised form 28 June 2010
Accepted 28 June 2010
Available online 31 July 2010

Keywords:
Cu,ZnSOD
$O_2^{\bullet-}$ and NO_2^- biosensor
CNT
Polypyrrole
Nanocomposite

ABSTRACT

A novel highly sensitive biosensor for the direct and simultaneous determination of superoxide anion radical ($O_2^{\bullet-}$) and nitrite (NO_2^-) was developed by incorporation of carbon nanotube (CNT) solubilized in nafion in polypyrrole (PPy) matrix on Pt electrode followed by immobilization of Cu,ZnSOD (SOD1) on it. The CNT/PPy nanocomposite electrode enhanced the immobilization of SOD1 and promoted the electron transfer of SOD1 minimizing its fouling effect. The surface morphological images of PPy and CNT–PPy nanocomposite on Pt electrode were obtained by scanning electron microscopy exhibiting highly microporous structures. The electrochemical behavior of the biosensor investigated by cyclic voltammetry revealed that the SOD1 immobilized electrode showed characteristic of SOD1 quasi-reversible redox peaks with a formal potential of +0.065 V vs. Ag/AgCl. The biosensor exhibited a linear response over the concentration range from 0.1 to 750 μM, with a detection limit of 0.1 ± 0.03 μM for $O_2^{\bullet-}$ and a corresponding linear range of 0.5–2000 μM, with a detection limit of 0.5 ± 0.025 μM for NO_2^-. In addition, the biosensor exhibited high sensitivity, good reproducibility and retained stability over 30 days. This modified electrode was quite effective not only in detecting $O_2^{\bullet-}$ and NO_2^- independently but also determining the concentration of $O_2^{\bullet-}$ and NO_2^- simultaneously *in vitro* and from cancer cells.

1. Introduction

Nitrite (NO_2^-) is a major oxidation product derived from NO that is produced by a wide variety of cell types by NO synthases (Knowles and Moncada, 1994). NO_2^- is also involved in the biosynthesis of NO (Stuehr and Marletta, 1985). There are several enzymatic and non-enzymatic pathways for the one-electron reduction of NO_2^- to NO. These include deoxyhemoglobin, deoxymyoglobin, xanthine oxidase and enzymes of the mitochondrial respiratory chain (Cosby et al., 2003; Shiva et al., 2007; Millar et al., 1998; Kozlov et al., 1999). NO_2^--derived NO has been suggested to possess several physiological functions such as vasodilation (Cosby et al., 2003) and protection against ischemia-reperfusion injury (Webb et al., 2004; Duranski et al., 2005). Similar to NO, $O_2^{\bullet-}$ play an important role in cell signaling and growth (Pacher et al., 2007). Inappropriate production of these radicals and their metabolites led to the development of various pathologies such as cancer, cardiovascular dysfunction, ischemia and neurodegenerative diseases (Halliwell and Gutteridge, 1986; Olanow, 1993; Smith et al., 1996; Samdani et al., 1997; Contestabile and Ciani, 2004). In order to understand the role of these in pathology, simultaneous monitoring of the local concentrations of NO_2^- and $O_2^{\bullet-}$ released from biological systems are increasingly important.

In the literature, NO_2^- and $O_2^{\bullet-}$ were determined by several independent methods. NO_2^- determination is mainly carried out by spectrophotometry (Griess reagent), ionic chromatography, capillary electrophoresis, and fluorescence methods (Moorcroft et al., 2001). Similarly, for the detection of $O_2^{\bullet-}$ indirect methods (Fridovich, 1997) such as spectrophotometric measurement (Haseloff et al., 1991), chemiluminescence method (Reichl et al., 2001), and electron spin resonance spectroscopy (Harbour and Hair, 1978) were used. However, these strategies are *ex situ* detection techniques with low sensitivity and poor selectivity. Among the centralized and sophisticated analytical systems, electrochemical techniques are proved to be powerful tools due to their advantages of simplicity, portability, inexpensive and fast analysis in combination with high selectivity.

Abbreviations: SOD1, Cu,ZnSOD; $O_2^{\bullet-}$, superoxide anion radical; NO_2^-, nitrite; NO_3^-, nitrate; PPy, polypyrrole; CNT, carbon nanotube; GA, glutaraldehyde; KO_2, potassium superoxide; PBS, phosphate buffer solution; DTPA, diethylenetriaminepentaacetic acid; H_2O_2, hydrogen peroxide; LPS, lipopolysaccharide; MEM, minimum essential medium; FBS, fetal bovine serum; SEM, scanning electron microscope; CV, cyclic voltammogram.

* Corresponding author.
E-mail address: ckaru2000@gmail.com (C. Karunakaran).

0956-5663/$ – see front matter © 2010 Elsevier B.V. All rights reserved.
doi:10.1016/j.bios.2010.06.063

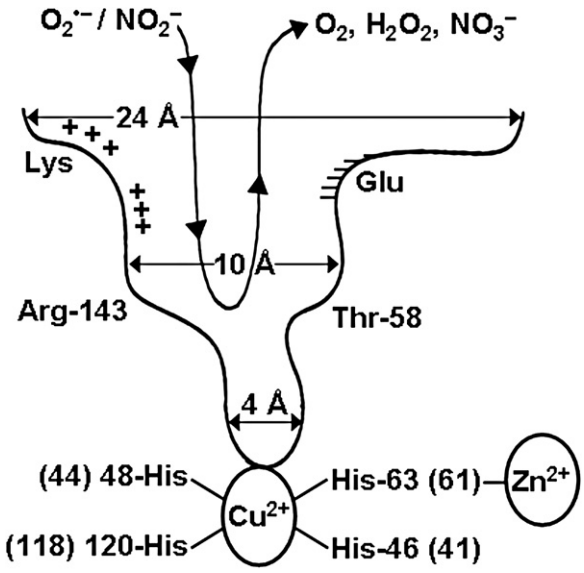

Scheme 1. Schematic illustration of active site channel of SOD1.

In the recent years, the enzymatic and non-enzymatic modified electrodes are used for the individual determination of $O_2^{\bullet-}$ and NO_2^-. NO_2^- biosensors have been widely reported using many heme proteins *viz*., hemoglobin, nitrite reductase, and myoglobin (Wu et al., 1997; Yang et al., 2005; Astier et al., 2005; Sun et al., 2009). These biosensors are mainly ascribed to the electroreductive reactions of NO_2^-. The reduction of NO_2^- yielded several products depending on the electrode conditions and the nature of the catalyst employed, while its anodic oxidation is a straightforward reaction, with NO_3^- being the final product (Caro et al., 2002). Hence, the anodic NO_2^- determination has attracted great attention because it offers several advantages especially with no interference. In contrast, the major limitations of cathodic determination of NO_2^- is due to interference from NO and O_2 (Wu et al., 1997; Yang et al., 2005; Astier et al., 2005).

For an individual electrochemical determination of $O_2^{\bullet-}$, SOD1, a selective scavenger of $O_2^{\bullet-}$ has been the best approach for the detection of $O_2^{\bullet-}$ compared to cyt *c* (Cooper et al., 1993; Lisdat et al., 1999) and hemin (Divisek and Kastening, 1975; Chen et al., 2000). Mostly, SOD1-immobilized electrodes have paved an elegant way to detect $O_2^{\bullet-}$. SOD1 show high rate constants, up to the order of 10^9 M^{-1} s^{-1}, and are distinguished by its highly uncommon specificity to $O_2^{\bullet-}$ (McCord and Fridovich, 1969; Fridovich, 1982; Oberley et al., 1985). Therefore, SOD1, a specific enzyme for $O_2^{\bullet-}$ dismutation, offers a great potential for the sensitive and selective quantification of $O_2^{\bullet-}$ in electrochemical biosensors. Here SOD1 is also employed for the electrocatalytic oxidation of NO_2^-, because of its active site channel is so narrow that it can allow selectively only small substrates (Scheme 1) (Karunakaran et al., 2004).

However enzyme immobilization on the electrode is a major hurdle. Recently, there has been wide interest in the field of conducting polymer-modified electrodes as it exhibited more porous structure (Lyons, 1994; Rajesh et al., 2010). Among the conducting polymers, polypyrrole (PPy) (Lyons, 1994) matrix increases the rates of reaction occurring at the electrode surface by mediating the electron transport and also the surface area. Further, carbon nanotubes (CNTs), have gained considerable interest in the field of electrochemical sensing devices with excellent sensitivity and fast response time owing to their unique structural, electronic, mechanical and chemical properties, and high surface area. It also enhances the electron transfer capability of enzyme-immobilized electrodes (Wang et al., 2003a; Cai and Chen, 2004). CNT has also reduced the overpotential of electrochemical oxidation/reduction reaction (Wang et al., 2003a; Cai and Chen, 2004). Recently, nafion, a polymer has been demonstrated to be particularly useful for preparing CNT-based electrodes because of its capability of confining the CNTs on the base electrodes and solubilizing the CNT in solution (Wang et al., 2003b; Gong et al., 2005).

So, in this study SOD1 immobilized on CNT–PPy nanocomposite electrode is made exhibiting high conductivity, biocompatibility and stability for the first time for the simultaneous electrochemical determination of $O_2^{\bullet-}$ and NO_2^- using the superoxide dismutase and nitrite oxidase activities of SOD1. These novel CNT–PPy nanocomposite electrodes provided microporous matrix for the enhanced immobilization of SOD1 and also facilitated the direct electron transfer between SOD1 and Pt electrode leading to very sensitive and selective determination of $O_2^{\bullet-}$ and NO_2^- simultaneously *in vitro* and generated from breast cancer cells.

2. Experimental

2.1. Reagents

Cu,ZnSOD (SOD1) from bovine erythrocytes was obtained from Roche Diagnostics, USA. Single wall carbon nanotubes were purchased from Carbon Solutions, Inc., CA. Pyrrole, KO_2, $NaNO_2$, diethylenetriaminepentaacetic acid (DTPA) and lipopolysaccharide (LPS) were purchased from Sigma Company (USA). MCF-7 breast cancer cells were obtained from ATCC. Pyrrole was used without purification.

2.2. Instrumentations

All electrochemical experiments were performed on CHI 2000A electrochemical workstation (CHI, USA) with a conventional three electrode system which consisted of an Ag/AgCl wire as reference electrode, a Pt wire as auxiliary or counter electrode, and a Pt electrode with SOD1 immobilized in PPy/CNT as the working electrode. The size of Pt wire working electrode was 0.5 mm in diameter. The morphological scanning electron microscope (SEM) images of CNT–PPy–Pt, PPy–Pt, and bare Pt electrodes were obtained using a FEI Quanta FEG 200-High Resolution Scanning Electron Microscope (FEI Co., Netherlands).

3. Methods

3.1. Construction of SOD1/CNT/PPy/Pt electrode

3.1.1. Pyrrole electropolymerization

Prior to electropolymerization, the electrode was polished with alumina powder (size 0.05 and 1.0 μm) until to get a highly shining surface, and washed twice with double distilled water. Finally, the electrode was cleaned in 1 M H_2SO_4 by cycling the potential from −200 to +1450 mV vs. Ag/AgCl until to attain reproducible cyclic voltammograms (CVs), and then washed with double distilled water. This pretreatment was employed before each electropolymerization. PPy films were electropolymerized onto the bare Pt electrode from deaerated solution of 0.4 M pyrrole, using 0.1 M KCl as supporting electrolyte, at the potential between 0.0 and +0.9 V vs. Ag/AgCl at a scan rate of 50 mV s^{-1}, for 10 complete cycles. The pyrrole polymerization was carried out under argon atmosphere at room temperature. The optimum of 10 cycles for pyrrole electropolymerization was used because of its increased conductivity and surface area as reported earlier (Razola et al., 2002) for the effective immobilization of SOD1/CNT.

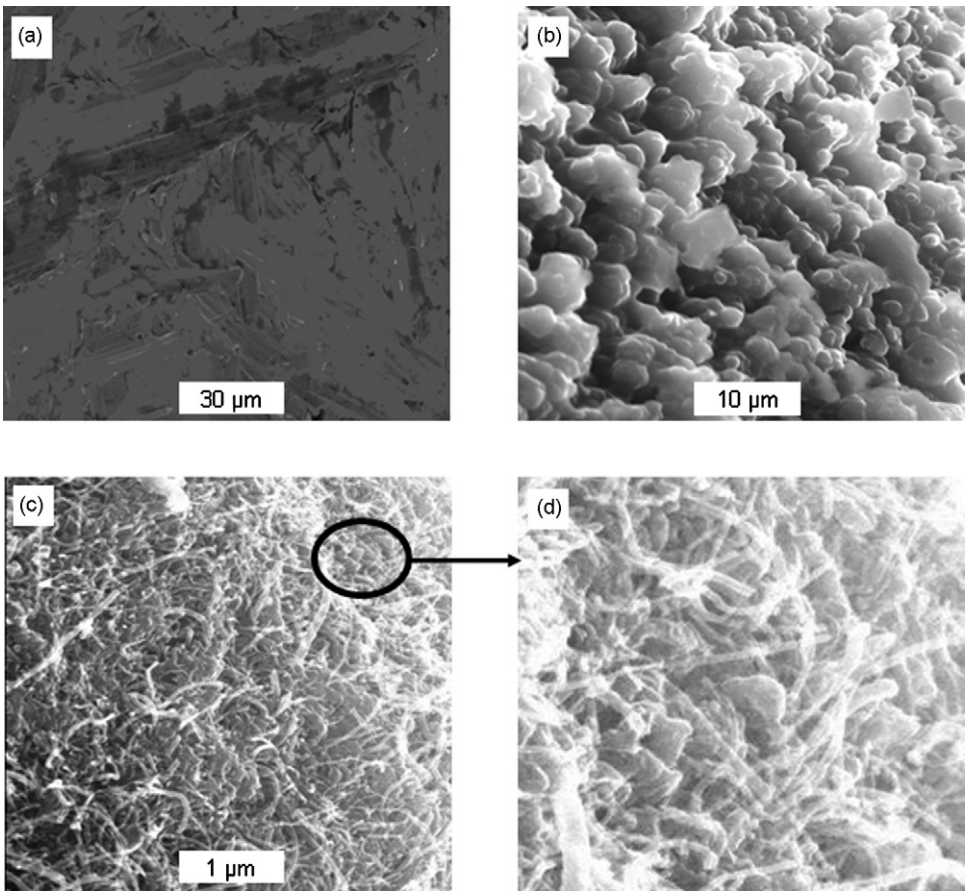

Fig. 1. SEM images of (a) bare Pt, (b) PPy–Pt, (c) CNT–PPy–Pt electrodes and d) enlarged the area as indicated in (c).

3.1.2. Construction of the CNT–PPy nanocomposite SOD1 biosensor

The CNT modified PPy/Pt electrode was prepared by the reported procedure (Wang et al., 2003b). In brief, 25 μL of CNT solution (1 ml of 0.5 wt% nafion–ethanol solution containing 2 mg of CNT) was dropped on PPy–Pt electrode surface, and then the solvent ethanol was evaporated in air to form a CNT–PPy nanocomposite. Then, 5 μL of SOD1 (0.2 g/mL) solution was immobilized onto CNT/PPy/Pt modified electrode by employing 5 μL of glutaraldehyde (GA) (2.5%) solution as cross-linking agent. After that, the electrode was left for at least 24 h at room temperature for efficient cross-linking. During this process, the SOD1 enzyme was entrapped on CNT/PPy/Pt. The preparation of these modified electrodes was reproducible, which could be confirmed from the cyclic voltammetric response and SEM of surface coverage of CNT, PPy and SOD1 enzymes. The amount of SOD1 immobilized on CNT/PPy/Pt was estimated by integrating the area of the cathodic peak of CV obtained in SOD1–CNT–PPy–Pt electrode compared to without SOD1 (Tian et al., 2002). The above constructed $O_2^{\bullet-}$ and NO_2^- biosensor is illustrated in Scheme S1(A) (See Supplementary Data). All the experiments were carried out at $27 \pm 0.5\,^{\circ}C$.

3.1.3. Cell culture

MCF-7 cells were grown in 10% minimum essential medium (MEM) containing 10% fetal bovine serum (FBS), L-glutamine (4 mmol/L), penicillin (100 units/mL), and streptomycin (100 μg/mL), and incubated at 37 °C in a humidified atmosphere of 5% CO_2 and 95% air. For $O_2^{\bullet-}$ and NO_2^- detection, cells were treated with 50 ng/mL of LPS for a period of 0–48 h.

4. Results and discussion

Recent advances in the development of amperometric biosensors became possible with the discovery that pyrrole can be electrochemically polymerized to give microporous structure for enhanced loading of enzymes (Mesaros et al., 1998) and CNT for their high conductivity, mechanical strength, large surface area and promoter of electron transfer process (Gong et al., 2005). Here, we have attempted to entrap CNT followed by SOD1 in the highly porous PPy matrix on the electrode surface without SOD1 denaturation. Further, the CNT–PPy nanocomposite retained the conductivity and electrocatalytic properties of the CNTs for electroanalytical applications. Similar to CNT, CNT–PPy nanocomposite has facilitated the direct electron transfer between the active site of SOD1 and the base electrode and also enhanced the loading of SOD1 to achieve high sensitivity for simultaneous determination of $O_2^{\bullet-}$ and NO_2^- levels in biological samples.

4.1. Electrochemical characterization of SOD1–CNT–PPy–Pt electrode

Figure S1 (See Supplementary Data) shows the typical CV of modified electrodes in 0.1 M PBS at pH 7.0. There were no peaks obtained on the CV range from −0.6 to +1.0 V at scan rate of 50 mV s^{-1} in PPy–Pt (Fig. S1a) and CNT–PPy–Pt electrodes (Fig. S1b). The CV of SOD1 immobilized in both PPy–Pt (Fig. S1c) and CNT–PPy–Pt electrode (Fig. S1d) exhibited quasi-reversible peaks with a formal potential of +0.065 V vs. Ag/AgCl. The formal redox potential of the Cu(I/II) complex moiety of SOD1 thus obtained is in agreement with the SOD1 observed in solution (data not shown)

and also with the previously published data for SOD1 (Ohsaka et al., 2002). The SOD1–CNT–PPy–Pt electrode (Fig. S1d) exhibited a twofold increase in current than that of SOD1 immobilized on PPy–Pt electrode (Fig. S1c). These results clearly demonstrate that the CNT–PPy nanocomposite well promoted the direct electron transfer between the SOD1 enzyme and Pt electrode and also provided the effective loading of SOD1. The well-defined quasi-reversible redox peaks due to the SOD1 and the current observed were stable; for instance, it remained essentially unchanged when the potential scan was repeated at 50 mV s^{-1} for 10 min. These data clearly suggested that the observed redox response is ascribable to the SOD1 confined on the CNT–PPy–Pt electrode.

The morphologies of CNT–PPy–Pt, PPy–Pt and bare Pt electrodes were investigated by SEM. The obtained morphological changes of the modified electrodes are exhibited in Fig. 1(a)–(d). In Fig. 1(b), the typical highly porous morphology of PPy on Pt electrode surface is shown. This high porous PPy matrix provided much larger surface area to entrap more CNT and SOD1 at the electrode surface. The incorporation of CNT in PPy film further exhibits highly microporous structure (Fig. 1c) thus increasing the effective surface area of the conducting polymeric film for SOD1 immobilization. The surface coverage of electroactive SOD1 in CNT–PPy nanocomposite is 1.26×10^{-9} mol cm^{-2}. This reveals that SOD1 is more effectively loaded on CNT–PPy nanocomposite electrode compared to PPy matrix.

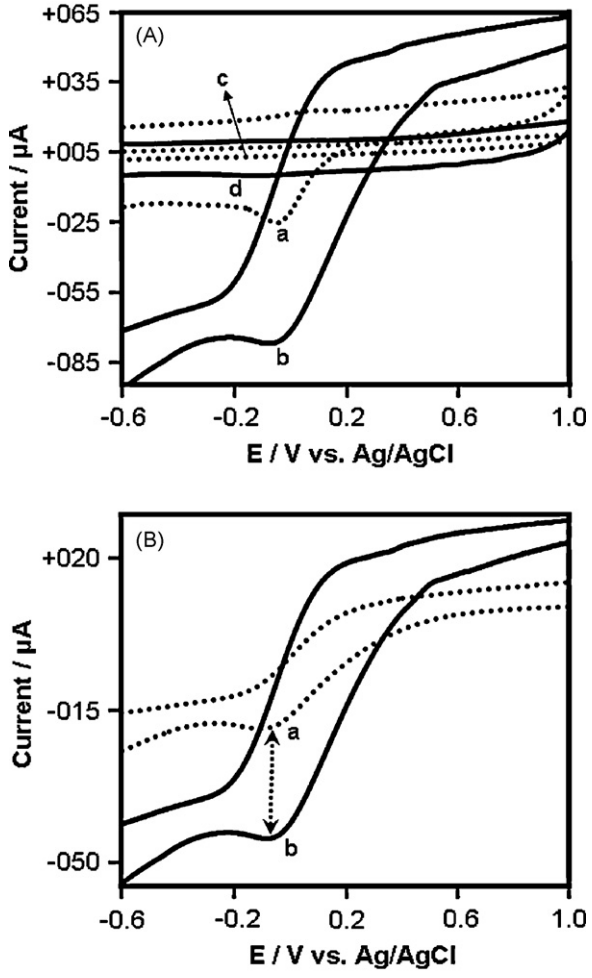

Fig. 2. (A) CVs obtained at SOD1–CNT–PPy–Pt and CNT–PPy–Pt electrodes (dotted) in the absence (a and c); (solid) in the presence (b and d) of 500 µM KO_2 solution in 0.1 M PBS (pH 7.0) containing 100 µM DTPA; scan rate: 50 mV s^{-1}. (B) Influence of CNT on the amperometric response of (a) SOD1–PPy–Pt and (b) SOD1–CNT–PPy–Pt electrodes to 250 µM KO_2 solution at scan rate of 50 mV s^{-1} in 0.1 M PBS (pH 7.0) containing 100 µM DTPA.

4.2. Electrochemical response to $O_2^{\bullet-}$

Fig. 2(A) compares the CV obtained at the SOD1–CNT–PPy–Pt and CNT–PPy–Pt electrodes in 0.1 M PBS (pH 7.0) in the absence and presence of $O_2^{\bullet-}$. Here, KO_2 was used to generate $O_2^{\bullet-}$. Fig. 2(A, a and c) shows the CV response of SOD1–CNT–PPy–Pt and CNT–PPy–Pt electrodes in the absence of $O_2^{\bullet-}$. In the presence of $O_2^{\bullet-}$, a significant increase in both the anodic and cathodic peak currents corresponding to the redox reaction of the SOD1 on the electrode is seen (Fig. 2A, b). Also the quasi-reversible peaks of SOD1 become reversible. However, such a redox response was not observed at the CNT–PPy–Pt electrode containing no SOD1 in the presence of $O_2^{\bullet-}$ (Fig. 2A, d). This suggests that the current response is due to the electrocatalytic redox reaction of $O_2^{\bullet-}$ with SOD1. Further, the observed current response due to only $O_2^{\bullet-}$ is evidenced from the fact that the external addition of 5 µM of SOD1 to the solution decreased the anodic and cathodic peak by 95%, because SOD1 effectively scavenged $O_2^{\bullet-}$ (data not shown). The obtained increase in the currents of anodic and cathodic peaks of the SOD1 immobilized in CNT–PPy–Pt electrode can be represented in Scheme S1(B) (See Supplementary Data). The bifunctional electrocatalytic activity of SOD1-based biosensor is effectively based on the inherent specificity of the SOD1 enzymes which catalyzes the dismutation of $O_2^{\bullet-}$ to O_2 and H_2O_2 *via* a cyclic redox reaction of its Cu(I/II) complex moiety (Scheme S1B). The following mechanism may explain the enhanced anodic oxidation current observed in Fig. 2(A).

$$\text{SOD1-Cu(I)} - e^- \rightarrow \text{SOD1-Cu(II)} \quad (1)$$

$$\text{SOD1-Cu(II)} + O_2^{\bullet-} \rightarrow \text{SOD1-Cu(I)} + O_2 \quad (2)$$

Similarly, the reduction current was enhanced in the cathodic scan according to the reactions

$$\text{SOD1-Cu(II)} + e^- \rightarrow \text{SOD1-Cu(I)} \quad (3)$$

$$\text{SOD1-Cu(I)} + O_2^{\bullet-} + H^+ \rightarrow \text{SOD1-Cu(II)} + H_2O_2 \quad (4)$$

Fig. 2(B) shows the effect of CNT on the current response of the biosensor to $O_2^{\bullet-}$. The CNT modified electrode exhibited a four-fold increase in the amperometric response in the presence of $O_2^{\bullet-}$ compared to the electrode without CNT.

4.3. Electrochemical response to NO_2^-

Recently, nitrite reductase, hemoglobin, and myoglobin have been widely used for NO_2^- biosensors (Wu et al., 1997; Yang et al., 2005; Astier et al., 2005; Sun et al., 2009). The electroreductive reactions of NO_2^- in these biosensors gave NO as a product causing interference by its reaction with oxygen. Hence, the anodic NO_2^- oxidation method using the nitrite oxidase activity of SOD1 was used here for the determination of NO_2^-. The nitrite oxidase activity exhibited by SOD1 is shown in Fig. 3(A). The CVs of the SOD1–CNT–PPy–Pt and CNT–PPy–Pt electrodes in 0.1 M PBS in the applied potential range from −0.6 to +1.0 V at a scan rate of 50 mV s^{-1} in the absence of NO_2^- are displayed in Fig. 3(A, a and c). Upon addition of 100 µM of NO_2^- into the 0.1 M PBS, a new irreversible anodic oxidation peak appeared at about +0.68 V (Fig. 3A,

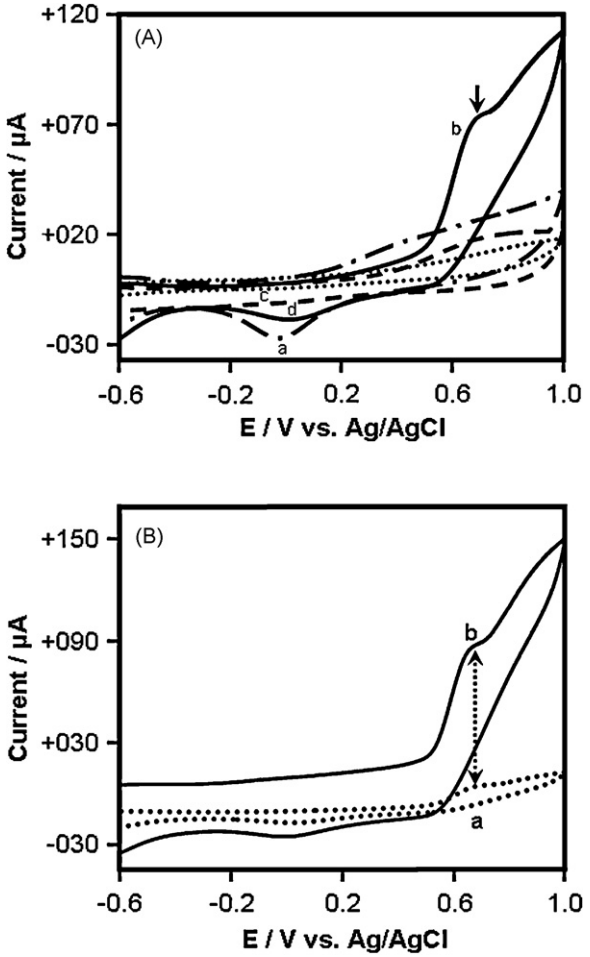

Fig. 3. (A) Typical CV response of SOD1–CNT–PPy–Pt and CNT–PPy–Pt electrodes (dotted) in the absence of (a) and (c); (solid) in the presence of (b) and (d) of 250 µM NO_2^- solution in 0.1 M PBS (pH 7.0) containing 100 µM DTPA; scan rate: 50 mV s^{-1} vs. Ag/AgCl. (B) Influence of CNT on the amperometric response of (a) SOD1–PPy–Pt and (b) SOD1–CNT–PPy–Pt electrodes to 500 µM NO_2^- solution at scan rate of 50 mV s^{-1} in 0.1 M PBS (pH 7.0) containing 100 µM DTPA.

b), which may be attributed to the oxidation of NO_2^- to NO_3^-. But, without SOD1 in the modified electrode under the same condition in the presence of NO_2^-, there was only a very small change at about +0.7 V observed (Fig. 3A, d). This study clearly demonstrates the electrocatalytic anodic oxidation of NO_2^- to NO_3^- exhibited by SOD1 immobilized on CNT–PPy–Pt and the equation of electrode reaction can be described as follows:

$$NO_2^- + H_2O \rightarrow NO_3^- + 2H^+ + 2e^- \quad (5)$$

The effect of CNT on the current response due to NO_2^- is shown in Fig. 3(B). It exhibits a remarkable increase in the amperometric response from the modified electrode consisting of CNT when compared to the electrode without CNT. Further with NO_2^- (100 µM), the increase in the anodic oxidation current observed at the SOD1–CNT–PPy–Pt electrode was fivefold greater than that of the CNT free SOD1–PPy–Pt electrode (Fig. 3B). It is clearly evident that the CNT–PPy nanocomposite facilitated the direct electron transfer between SOD1 and the base electrode.

4.4. Linearity, stability, reproducibility and selectivity

Typical CVs obtained for several concentrations of KO_2 in 0.1 M PBS were measured using the $O_2^{\bullet-}$ biosensor at 50 mV s^{-1} and are shown in Fig. 4(A). The observed cathodic currents vs. $O_2^{\bullet-}$ concentrations are plotted as shown in Fig. 4(B). The calibration curve for SOD1–CNT–PPy–Pt electrode thus obtained exhibits a linear range for the $O_2^{\bullet-}$ concentrations from 0.1 to 750 µM ($r^2 = 0.9948$) with a detection limit of 0.1 ± 0.03 µM and sensitivity of 0.19 ± 0.003 µA μM^{-1} cm^{-2}. Without CNT, the sensitivity of SOD1–PPy–Pt electrode for $O_2^{\bullet-}$ determination is only 0.016 ± 0.005 µA μM^{-1} cm^{-2}. Recently, we also reported the electrochemical determination of $O_2^{\bullet-}$ using SOD1 immobilized on self-assembled cysteine monolayer on gold nanoparticles in PPy matrix on Pt electrode (Rajesh et al., 2010). However, the present SOD1–CNT–PPy–Pt electrode exhibited excellent electroanalytical performance, for instance, wider linear detection range and high sensitivity compared to the other reported $O_2^{\bullet-}$ biosensors (Table S1) (See Supplementary Data).

Fig. 5(A) displays the typical catalytic current response at the SOD1 immobilized CNT–PPy–Pt electrode with the increase in the concentration of NO_2^- at 50 mV s^{-1}. A progressive increase in the current response was observed at +0.68 V with the increase in the concentration of NO_2^- from 0 to 2000 µM as shown in inset Fig. 5A. The anodic oxidation peak currents measured at the modified electrode were almost linearly related to the concentration of NO_2^- in the range of 0.5–2000 µM and the detection limit was 0.5 ± 0.025 µM, with a sensitivity of 0.2 ± 0.002 µA μM^{-1} cm^{-2}. Without CNT, the SOD1–PPy–Pt electrode exhibited low sensitivity (0.012 ± 0.003 µA μM^{-1} cm^{-2}) for NO_2^-. The characteristic of the present NO_2^- biosensor along with the other reported modified electrodes for comparison are listed in Table S2 (See Supplementary Data). It reveals that the detection limit and the sensitivity of

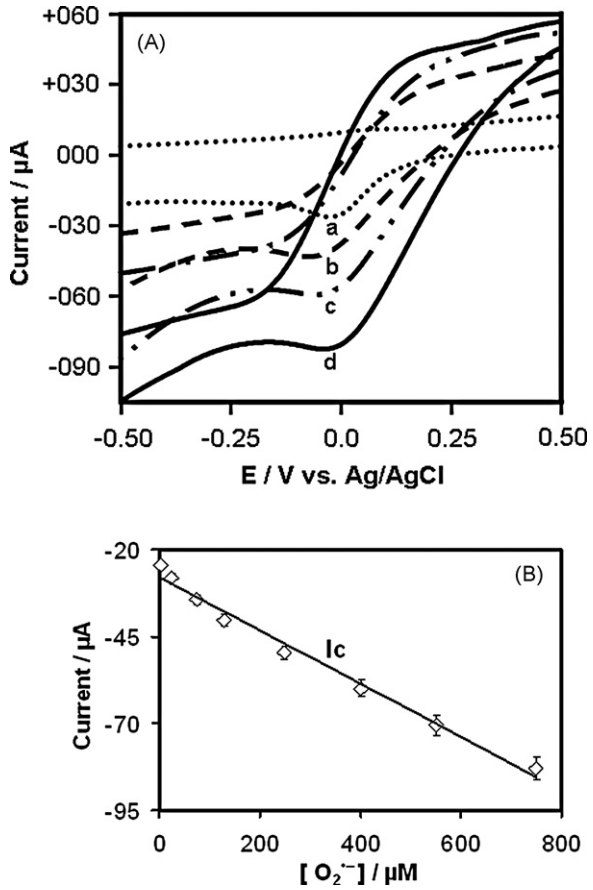

Fig. 4. (A) Typical CV response of SOD1–CNT–PPy–Pt electrode in 0.1 M PBS containing (a) control, (b) 50 µM, (c) 250 µM, and (d) 750 µM $O_2^{\bullet-}$ at scan rate of 50 mV s^{-1}. (B) A linear calibration plot of cathodic peak currents against $O_2^{\bullet-}$ concentrations. Each point represents the mean (±0.03 SD) of three measurements.

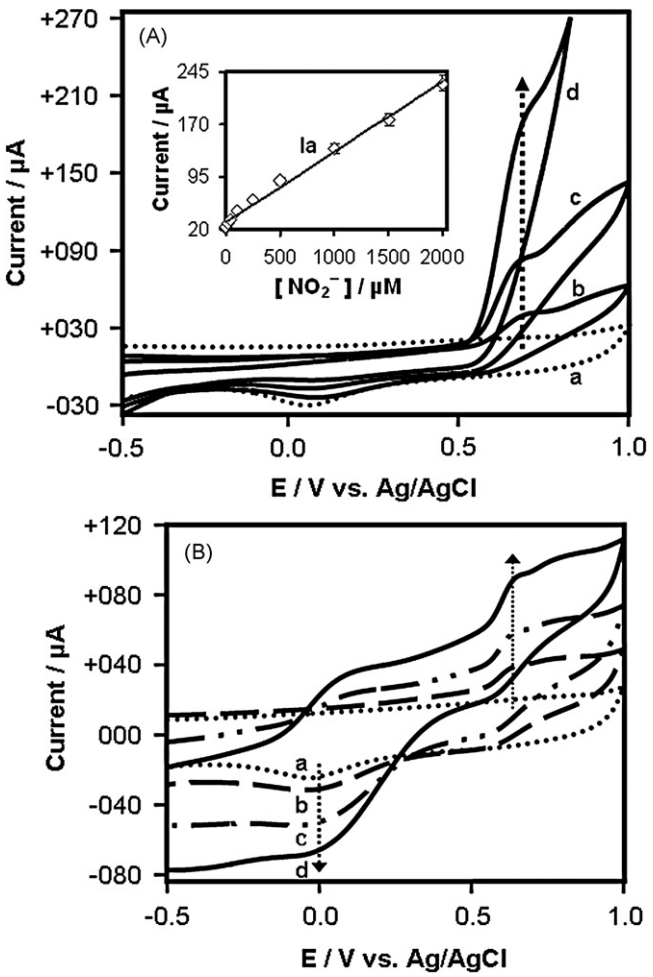

Fig. 5. (A) CVs of SOD1–CNT–PPy–Pt electrode in 0.1 M PBS containing (a) control, (b) 100 μM, (c) 500 μM, and (d) 2000 μM NO_2^- at a scan rate of 50 mV s^{-1}. A linear calibration plot of anodic peak currents against NO_2^- concentrations (inset figure). Each point represents the mean (±0.025 SD) of three measurements. (B) Simultaneous electrochemical response of SOD1–CNT–PPy–Pt electrode on (a) control, (b) 50 μM $O_2^{\bullet-}$ + 100 μM NO_2^-, (c) 300 μM $O_2^{\bullet-}$ + 250 μM NO_2^-, and (d) 550 μM $O_2^{\bullet-}$ + 600 μM NO_2^- at scan rate of 50 mV s^{-1}.

the SOD1 modified electrode are much better than other modified electrodes (Table S2). The data suggests that the SOD1 immobilized CNT–PPy nanocomposite based biosensor could be potentially used for monitoring the concentration of NO_2^- sensitively and selectively. The reproducibility of the present method for the determinations of $O_2^{\bullet-}$ and NO_2^- were investigated in 0.1 M PBS containing 100 μM $O_2^{\bullet-}$ and 50 μM NO_2^- by repetitive determination of $O_2^{\bullet-}$ and NO_2^- in triplicate. The results showed good reproducibility of the modified electrode, with a relative standard deviation of 3.8% and 3.2% for $O_2^{\bullet-}$ and NO_2^- respectively. For studying the stability of the biosensor, the anodic and cathodic responses for $O_2^{\bullet-}$ and NO_2^- were recorded three times daily and the current responses were found to be constant for at least 30 days. The good analytical properties of the biosensor, such as low detection limit, long term stability, and high sensitivity, eventually have shown a great promise for simultaneous measurement of $O_2^{\bullet-}$ and NO_2^- in biological samples.

4.5. Simultaneous determination of $O_2^{\bullet-}$ and NO_2^-

Fig. 5(B) exhibits the CVs obtained by simultaneously increasing the concentrations of $O_2^{\bullet-}$ from 0 to 550 μM and NO_2^- from 0 to 600 μM. From the results, it is clearly obvious that increases in the anodic/cathodic peak currents at the potential of +0.1 V/−0.035 V due to $O_2^{\bullet-}$ and anodic peak current at the potential of +0.68 V due to NO_2^- were observed with the increasing $O_2^{\bullet-}$ and NO_2^- concentrations. The selective electrocatalytic reactions of SOD1 with $O_2^{\bullet-}$ and NO_2^- perhaps explained due its narrow positively charged active site channel (Scheme 1). These data clearly demonstrates that $O_2^{\bullet-}$ and NO_2^- levels were simultaneously determined using the SOD1 immobilized on CNT–PPy nanocomposite electrode.

4.6. Measurement of $O_2^{\bullet-}$ and NO_2^- released from MCF-7 cancer cells

Earlier it has been shown that NO_2^- a stable end product of NO, and $O_2^{\bullet-}$ are generated by breast cancer cells when exposed to HMG-CoA reductase inhibitors (Kotamraju et al., 2007). In this study, we attempted to measure NO_2^- and $O_2^{\bullet-}$ simultaneously by using our newly developed biosensor in MCF-7 cells stimulated with LPS. Figure S2 (solid line) (See Supplementary Data) shows the simultaneous amperometric monitoring of $O_2^{\bullet-}$ and NO_2^- release from LPS treated MCF-7 cancer cells. After 24 h stimulation by 50 ng/mL of LPS, the cathodic peak current at the potential, −0.035 V for $O_2^{\bullet-}$ and the anodic peak current at the potential, +0.68 V for NO_2^- were clearly seen. However at 48 h duration, the peak current due to $O_2^{\bullet-}$ increased but the peak current due to NO_2^- remained constant. The $O_2^{\bullet-}$ (0.1 ± 0.02 μM) and NO_2^- (4.2 ± 0.015 μM) levels generated from the stimulated cancer cells at 48 h were determined from the calibration plots (Figs. 4B and 5A inset) which are in agreement with the reference methods (Kotamraju et al., 2007; Wang et al., 2004).

5. Conclusions

We report here for the first time SOD1 immobilized on CNT–PPy nanocomposite based biosensor for the simultaneous detection and measurement of $O_2^{\bullet-}$ and NO_2^- using its superoxide dismutase and nitrite oxidase activities. This study demonstrates that CNT–PPy nanocomposites enhanced the loading as well as promoted the direct electron transfer process between the active site of SOD1 and the base electrode resulting in very high sensitivity and long term stability due to its biocompatibility. The synergistic effect of nanocomposite containing PPy and CNT resulted in superior electrochemical determination of $O_2^{\bullet-}$ and NO_2^- in comparison to the other biosensors. This study has further demonstrated that simultaneous monitoring of $O_2^{\bullet-}$ and $NO_2^{\bullet-}$ generated from cell culture model systems could be achieved in real time using the direct electrochemical biosensor system.

Acknowledgements

Thanks are due to the Managing Board, VHNSN College, Virudhunagar and DIPAS-DRDO, New Delhi for funding/providing facilities to carry out the research in the Biomedical Research Laboratory, VHNSN College, Virudhunagar, Tamil Nadu, India. Ramanujan fellowship to Dr. Srigiridhar Kotamraju from DST, India is greatly acknowledged.

Appendix A. Supplementary data

Supplementary data associated with this article can be found, in the online version, at doi:10.1016/j.bios.2010.06.063.

References

Astier, Y., Canters, G.W., Davis, J.J., Hill, H.A.O., Verbeet, M.P., Wijma, H.J., 2005. ChemPhysChem 6, 1114–1120.

Bard, A.J., Faulkner, L.R., 1980. Electrochemical Methods, Fundamentals and Applications. Wiley, New York.
Cai, C.-X., Chen, J., 2004. Anal. Biochem. 325, 285–292.
Campanella, L., Persi, L., Tomassetti, M., 2000. Sens. Actuators B 68, 351–359.
Caro, C.A., Bedioui, F., Zagal, J.H., 2002. Electrochim. Acta 47, 1489–1494.
Chen, J., Wollenberger, U., Lisdat, F., Ge, B., Scheller, F.W., 2000. Sens. Actuators B 70, 115–120.
Contestabile, A., Ciani, E., 2004. Neurochem. Int. 45, 903–914.
Cooper, J.M., Greenough, K.R., McNeil, C.J., 1993. J. Electroanal. Chem. 347, 267–275.
Cosby, K., Partovi, K.S., Crawford, J.H., Patel, R.P., Reiter, C.D., Martyr, S., Yang, B.K., Waclawiw, M.A., Zalos, G., Xu, X., Huang, K.T., Shields, H., Kim-Shapiro, D.B., Schechter, A.N., Cannon 3rd, R.O., Gladwin, M.T., 2003. Nat. Med. 9, 1498–1505.
Deng, Z., Rui, Q., Yin, X., Liu, H., Tian, Y., 2008. Anal. Chem. 80, 5839–5846.
Di, J., Bi, S., Zhang, M., 2004. Biosens. Bioelectron. 19, 1479–1486.
Divisek, J., Kastening, B., 1975. J. Electroanal. Chem. 65, 603–621.
Doherty, A.P., Forster, R.J., Smyth, M.R., Vos, J.G., 1991. Anal. Chim. Acta 255, 45–52.
Duranski, M.R., Greer, J.J., Dejam, A., Jaganmohan, S., Hogg, N., Langston, W., Patel, R.P., Yet, S.F., Wang, X., Kevil, C.G., Gladwin, M.T., Lefer, D.J., 2005. J. Clin. Invest. 115, 1232–1240.
Fridovich, I., 1982. In: Oberley, L.W. (Ed.), Superoxide Dismutase, vol. 1. CRC Press, Boca Raton, FL (Chapter 3).
Fridovich, I., 1997. J. Biol. Chem. 272, 18515–18517.
Geng, R., Zhao, G., Liu, M., Li, M., 2008. Biomaterials 29, 2794–2801.
Gong, K., Yan, Y., Zhang, M., Su, L., Xiong, S., Mao, L., 2005. Anal. Sci. 21, 1383–1393.
Gong, K., Dong, Y., Xiong, S., Chen, Y., Mao, L., 2004. Biosens. Bioelectron. 20, 253–259.
Halliwell, B., Gutteridge, J.M.C., 1986. Arch. Biochem. Biophys. 246, 501–514.
Harbour, J.R., Hair, M.L., 1978. J. Phys. Chem. 82, 1397–1399.
Haseloff, R.F., Ebert, B., Wischnewsky, G.G., 1991. Anal. Chim. Acta 243, 221–225.
Huang, X., Li, Y., Chen, Y., Wang, L., 2008. Sens. Actuators B 134, 780–786.
Karunakaran, C., Zhang, H., Crow, J.P., Antholine, W.E., Kalyanaraman, B., 2004. J. Biol. Chem. 279 (31), 32534–32540.
Kozlov, A.V., Staniek, K., Nohl, H., 1999. FEBS Lett. 454, 127–130.
Knowles, R.G., Moncada, S., 1994. Biochem. J. 298, 249–258.
Lisdat, F., Ge, B., Forster, E.E., Reszka, R., Scheller, F.W., 1999. Anal. Chem. 71, 1359–1365.
Lyons, M.E.G., 1994. Analyst 119, 805–826.
McCord, J.M., Fridovich, I., 1969. J. Biol. Chem. 244, 6094–6099.
Mesaros, S., Vankova, Z., Grunfeld, S., Mesarosova, A., Malinski, T., 1998. Anal. Chim. Acta 358, 27–33.
Millar, T.M., Stevens, C.R., Benjamin, N., Eisenthal, R., Harrison, R., Blake, D.R., 1998. FEBS Lett. 427, 225–228.
Moorcroft, M.J., Davis, J., Compton, R.G., 2001. Talanta 54, 785–803.
Oberley, L.W. (Ed.), 1985. Superoxide Dismutase, vol. 3. CRC Press, Boca Raton, FL, pp. 45–82.
Ohsaka, T., Tian, Y., Shioda, M., Kasahara, S., Okajima, T., 2002. Chem. Commun., 990–991.
Olanow, C.W., 1993. Trends Neurosci. 16, 439–444.
Pacher, P., Beckman, J.S., Liaudet, L., 2007. Physiol. Rev. 87 (1), 315–424.
Rajesh, S., Arivudainambi, U.S.E., Rajasingh, S., Rajendran, A., Srigiridhar, Kotamraju, Karunakaran, C., 2010. Sensor Lett. 8 (4), 613–621.
Razola, S.S., Lopez Ruiz, B., Mora Diez, N., Mark Jr., H.B., Kauffmann, J.-M., 2002. Biosens. Bioelectron. 17, 921–928.
Reichl, S., Vocks, A., Petkovic, M., Schiller, J., Arnhold, J., 2001. Free Radical Res. 35, 723–733.
Samdani, A.F., Dawson, T.M., Dawson, V.L., 1997. Stroke 28, 1283–1288.
Sljukic, B., Banks, C.E., Crossley, A., Compton, R.G., 2007. Anal. Chim. Acta 587, 240–246.
Shiva, S., Huang, Z., Grubina, R., Sun, J., Ringwood, L.A., MacArthur, P.H., Xu, X., Murphy, E., Darley-Usmar, V.M., Gladwin, M.T., 2007. Circ. Res. 100, 654–661.
Smith, M.A., Sayre, L.M., Monnier, V.M., Perry, G., 1996. Trends Neurosci. 18, 172–176.
Song, M.I., Bier, F.F., Scheller, F.W., 1995. Bioelectrochem. Bioenerg. 38, 419–422.
Srigiridhar Kotamraju, Williams, C.L., Kalyanaraman, B., 2007. Cancer Res. 67, 7386–7394.
Stuehr, D.J., Marletta, M.A., 1985. PNAS 82, 7738–7742.
Sun, W., Li, X., Wang, Y., Li, X., Zhao, C., Jiao, K., 2009. Bioelectrochemistry 75, 170–175.
Tian, Y., Shioda, M., Kasahara, S., Okajima, T., Mao, L., Hisabori, T., Ohsaka, T., 2002. Biochim. Biophys. Acta 1569, 151–158.
Wang, J., Deo, R.P., Poulin, P., Mangey, M., 2003a. J. Am. Chem. Soc. 125, 14706–14708.
Wang, J., Musameh, M., Lin, Y., 2003b. J. Am. Chem. Soc. 125, 2408–2409.
Wang, S., Konorev, E.A., Kotamraju, S., Joseph, J., Kalivendi, S., Kalyanaraman, B., 2004. J. Biol. Chem. 279, 25535–25543.
Webb, A., Bond, R., McLean, P., Uppal, R., Benjamin, N., Ahluwalia, A., 2004. PNAS 101, 13683–13688.
Wu, Q., Storrier, G.D., Parients, F., Wang, Y., Shapleigh, J.P., Abruna, H.D., 1997. Anal. Chem. 69, 4856–4863.
Yang, W., Bai, Y., Li, Y., Sun, C., 2005. Anal. Bioanal. Chem. 382, 44–50.